

# Seasonal cycle of ~~desertie~~-~~desert~~ aerosols in West Africa : Analysis of the Coastal transition with passive and active sensors

Habib Senghor <sup>1</sup>, Éric Machu <sup>1,2</sup>, Frédéric Hourdin <sup>3</sup>, and Amadou Thierno Gaye <sup>1</sup>

<sup>1</sup>Laboratoire de Physique de l'Atmosphère et de l'Océan Siméon-Fongang (LPAO-SF), École Supérieure Polytechnique (ESP) de l'Université Cheikh Anta Diop de Dakar (UCAD), Sénégal

<sup>2</sup>Laboratoire de Physique des Océans (LPO), Institut Universitaire Européen de la Mer (IUEM), Brest, France

<sup>3</sup>Laboratoire de Météorologie Dynamique (LMD), CNRS/IPSL/UMPC, Paris, France

*Correspondence to:* H. Senghor (habib.senghor@ird.fr)

1 **Abstract.** The impact of ~~desertie~~-~~desert~~ aerosols on climate, atmospheric processes and the environment is still debated in the  
2 scientific community. The extent of their influence remains to be determined and particularly requires a better understanding  
3 of the variability of their distribution. In this work, we studied the variability of these aerosols in West Africa using different  
4 types of satellite observations. SeaWiFS ~~and OMI~~ ([Sea-Viewing Wide Field-of-View Sensor](#)) and [OMI \(Ozone Monitoring](#)  
5 [Instrument\)](#) data have been used to characterize the spatial distribution of mineral aerosols from their optical and physical  
6 properties over the period 2005-2010. In particular, we focused on the variability of the transition between the West African  
7 continent and the Eastern Atlantic Ocean. Data provided by the Lidar scrolling CALIOP ([Cloud-Aerosol Lidar with Orthogonal](#)  
8 [Polarization](#)) onboard the satellite CALIPSO (Cloud Aerosol Lidar and Infrared Pathfinder Satellite Observations) for the  
9 period 2007-2013 were then used to assess the seasonal variability of the vertical distribution of ~~desertie~~-~~desert~~ aerosols.  
10 We first obtained a good representation of Aerosol Optical Depth (AOD) and Single Scattering Albedo (SSA) by satellites  
11 (~~SeaWiFS and OMI ,respectively~~) [respectively](#) in comparison with AERONET estimates, both above the continent and the  
12 ocean. Dust occurrence frequency is higher in spring and boreal summer. In spring, the highest occurrences are located between  
13 the surface and 3 km above sea level, while in summer the highest occurrences are between 2 and 5 km altitude. The vertical  
14 distribution given by CALIOP also highlights an abrupt change at the coast from spring to fall with a layer of ~~desertie~~-~~desert~~  
15 aerosols confined in an atmospheric layer uplifted from the surface of the ocean. This uplift of the aerosol layer above the ocean  
16 contrasts with the winter season during which mineral aerosols are confined in the atmospheric boundary layer. Radiosondes  
17 at Dakar Weather Station (17.5°W, 14.74°N) provide basic thermodynamic variables which partially give causal relationship  
18 between the layering of the atmospheric circulation over West Africa and their aerosol contents throughout the year. A SSA  
19 increase is observed in winter and spring at the transition between the continent and the ocean. The analysis of mean NCEP  
20 ([National Center for Environmental Prediction](#)) winds at 925 hPa between 2000 and 2012 suggest a significant contribution of  
21 coastal sand sources from Mauritania in winter which would increase SSA over the ocean.

## 22 1 Introduction

23 The Sahara is the largest source of mineral aerosols in the world, with a contribution of almost 40% compared to the overall  
24 emissions from natural sources (Ramanathan et al., 2001; Tanaka et al., 2005). ~~These minerals and desert aerosols are emitted~~  
25 ~~in arid and semi-arid North Africa and transported across the Atlantic Ocean to the American continent, the Caribbean islands,~~  
26 ~~Florida (Chiapello et al., 1995; Dunion and Marron, 2008), South America (Prospero et al., 1981; Liu et al., 2008, 2012) and~~  
27 ~~North America (Tsamalis et al., 2013).~~ The mineral dust aerosols emitted from the Sahara desert can be transported over long  
28 distances in the atmosphere and can be detected as far as Americas (Prospero et al., 1981; Swap et al., 1992; Formenti et al., 2001; Kaufman  
29 Mediterranean region (Bergametti et al., 1989; Moulin, 1997; Ansmann et al., 2003) and Asia (Ganor and Mamane, 1982; Israelevich et al.  
30 But here, the study of dust transport focuses on the main corridor of their transport Westward Africa (Formenti et al., 2001).  
31 They play a very important role on the climate and the various processes involved in the climate system (Kaufman et al.,  
32 2005; Teller and Levin, 2006; Stith et al., 2009) through their direct impact in the visibility, in the infrared (Sokolik and  
33 Toon, 1999) or the earth radiation budget (Andreae et al., 1996; Solomon, 2007) which is still poorly known. The difficulty  
34 of understanding the impact of aerosols on the Earth's radiation balance is due to the large spatial and temporal variability  
35 of their concentration and composition in the atmosphere. The mineral particles suspended in the atmosphere come from dif-  
36 ferent sources and have a nature similar to the nature of the soil from which they arise (Claquin et al., 1999; Formenti et al.,  
37 2008) with a broad spectrum of particle sizes ranging between 0.01 ~~and 100 micrometers (Wagener, 2008)~~  $\mu\text{m}$  and 300  $\mu\text{m}$   
38 (Wagener, 2008; Ryder et al., 2013). Their impact on the marine ecosystem and particularly on oceanic primary production  
39 (Duce and Tindale, 1991; Baker et al., 2003; Mills et al., 2004; Jickells et al., 2005; Mahowald et al., 2009) remains still  
40 uncertain and difficult to assess because of the composition of these particles and of physico-chemical processes affecting  
41 them ( e.g., Friese et al., 2016). Mineral dust deposition also have a negative impact on human health and are responsible for  
42 meningitis epidemics or cardiac diseases (Thomson et al., 2006; Martiny and Chiapello, 2013; Diokhane et al., 2016; Prospero  
43 et al., 2005; Griffin, 2007).

44 ~~The desert aerosols and their large-scale transport began to be studied in the 90s.~~ Although the transport of mineral dust across  
45 the Atlantic Ocean started to be investigated in the 1960s, it started to be studied from satellite observations (~~?Moulin, 1997~~) since  
46 1970s (Kaufman et al., 2005; Taghavi and Asadi, 2008). Passive sensors have the advantage of providing daily data on the state  
47 of the atmosphere with good spatial and temporal coverage. The satellite products have improved our knowledge of the source  
48 regions and dust transport pathways in recent years (~~Engelstaedter et al., 2006~~) (Engelstaedter et al., 2006; Schepanski et al., 2007, 2009b,  
49 However, studies of their spatial and temporal variability are mainly based on indices such as the Aerosol Optical Depth (AOD)  
50 or the Aerosol Index (AI) which provide vertically integrated information on the Atmospheric atmospheric aerosol contents  
51 (passive space derived observations: (~~Cakmur et al., 2001; Chiapello and Moulin, 2002; Kaufman et al., 2005; Engelstaedter et al., 2006; S~~  
52 ~~These satellite products also present some limitations since they are unable to differentiate aerosols and particularly those from~~  
53 ~~desertic origin.~~ Cakmur et al. (2001); Chiapello and Moulin (2002); Kaufman et al. (2005); Engelstaedter et al. (2006); Schepanski et al. (  
54 Moreover AOD estimated by satellite integrates the contribution of every kind of particles and this latter estimation also  
55 depends on the altitude at which aerosols are located. Based on perturbations induced by the Rayleigh scattering in the

56 detection of absorbing aerosols, Chiapello et al. (1999) showed that TOMS AI is more sensitive to aerosols present at high  
57 altitude than at low altitude. In other words the signal changes with the height of the aerosol plume for a given aerosol con-  
58 tent(~~Chiapello et al., 1999~~).

59 Recently, the vertical structure of the ~~SAL~~ Saharan Air Layer (SAL) has been analyzed from CALIPSO satellite observations.  
60 The vertical ~~diseconnection-discontinuity~~ of dust layers between land and ocean strongly impacts the atmospheric deposition  
61 rates of mineral matters (Schepanski et al., 2009a) and dust concentration at the oceanic surface which has important conse-  
62 quences on the primary biological productivity of surface waters (Martin, 1992; Aristegui et al., 2009).

63 In boreal summer, ~~the Saharan Air Layer (SAL)~~ SAL is characterized by hot, dry air, very dust-laden and is located between  
64 10°N and 25°N (Dunion and Marron, 2008; Tsamalis et al., 2013). This SAL is marked by very strong potential temperatures  
65 up to 40°C and a radon presence (radon-222) indicating the desert origin of air masses (Carlson and Prospero, 1972).

66 In winter, the SAL is characterized by the transport of dust containing chemical elements such as aluminum (Al), silicon (Si),  
67 iron (Fe), titanium (Ti) and manganese (Mn) ( e.g., ~~Ben-Ami et al., 2010~~ Formenti et al., 2001; Ben-Ami et al., 2010 ) and is  
68 located between 5°N and 10°N ( e.g., Tsamalis et al., 2013). ~~The Some of~~ studies relating aerosols to their transport are gener-  
69 ally a simple description of the vertical distribution of aerosols in the SAL (Generoso et al., 2008; Liu et al., 2008; Ben-Ami  
70 et al., 2009; Braun, 2010; Yu et al., 2010; Adams et al., 2012; Ridley et al., 2012; Yang et al., 2012) or a description of the  
71 seasonality of the SAL in connection with large-scale dynamics (Liu et al., 2012; Tsamalis et al., 2013). However, the dust field  
72 campaigns, AMMA, SAMMUM-1 and 2, FENNEC or SALTRACE (see Table 1) of Weinzierl et al., (2016) carried out in West  
73 Africa and over the Atlantic Ocean improved our understanding of dust-dynamics interactions. During SALTRACE, a linear  
74 depolarization ratio of particles and a relative humidity threshold of 50% were used for differentiating different types of aerosol  
75 (Weinzierl et al., 2016) . Authors showed that sea salt aerosol were restricted to the lower layer superposed by biomass-dust  
76 mixtures. They also showed that the altitude of the mineral dust layer decreased westward. The effects of small-scale dynamics  
77 and thermodynamics for controlling the vertical structure of desert aerosols in coastal West Africa remain unknown, and efforts  
78 made in this direction are restricted to very sporadic case studies (Gamo, 1996; Reid et al., 2002; Petzold et al., 2011).

79 In this study, in-situ and satellite observations are used to describe the seasonal time-scale of mineral dust distribution. We first  
80 used complementary information, provided by ~~Sea-viewing Wide Field-of-View Sensor (SeaWiFS) and Ozone Monitoring Instrument~~  
81 ~~(OMI) which deliver optical (AOD: Aerosol Optical Depth; SSA: Single Scattering Albedo) and physical (AE: Angstrom~~  
82 ~~Exponent) properties of desertie~~ SeaWiFS and OMI which deliver extensive (AOD) and intensive (SSA, AE) parameters of  
83 desert aerosols, to analyse the spatial variability of the ~~desertie~~ desert aerosol dust. Then we used CALIOP lidar on board  
84 CALIPSO to investigate the vertical distribution of these ~~desertie~~ desert aerosols.

85 We finally analyze meteorological data to explain the impact of the atmospheric variables on the seasonal cycle of the vertical  
86 distribution of ~~desertie~~ desert aerosols at the transition zone between the continent and the ocean. We conclude the present work  
87 by summarizing all the results which are reflecting our common knowledge on mineral dust discrimination and spatio-temporal  
88 distribution.

## 89 2 Methodology and Data

### 90 2.1 AEROSOL ROBOTIC NETWORK (AERONET)

91 We first used data of AOD from AERONET between January 2005 and December 2010. AERONET is a global network  
92 of in-situ observations developed by the NASA Earth Observing System (NASA's EOS) (Dubovik et al., 2000). AERONET  
93 consists of solar photometers Cimel providing measures of AOD every 15 minutes, refractive index and also allows inver-  
94 sions such as particle size distribution of aerosols and single scattering albedo (SSA) at 440nm, 670nm, 870nm and 1020nm  
95 wavelengths (Holben et al., 1998) with an accuracy of  $\pm 0.01$  (Slutsker and Kinne, 1999; Dubovik et al., 2000; Holben et al.,  
96 2001). This uncertainty is inherent in the algorithm inversion used to retrieve aerosol characteristics. Some approximations  
97 are used in the numerical inversion algorithm which produce errors named relative errors having a standard deviation of 0.01  
98 (Dubovik et al., 2000). AERONET's SSA are computed for favorable atmospheric conditions (AOD 440 nm > 0.4 and solar  
99 zenith angle >45°) using an algorithm which performs almucantar inversions (Jethva et al., 2014). These data are used to vali-  
100 date remotely sensed AOD and SSA measurements. AERONET is available under three different products: Level 1.0, 1.5 and  
101 2.0. In this study, we use Level 1.5 product for Cape Verde, due to a lack of sufficient Level 2 data, for this station and Level  
102 2.0 for the other stations. Concerning the temporal resolution of AERONET observations, we compute a "daily" mean based  
103 upon data collected between 10am and 3pm in order to use observations collected during the same time window as satellite  
104 overpass. We then use this 10am-3pm daily averages to compute monthly 10am-3pm AOD.

### 105 2.2 Sea-viewing Wide Field-of-view Sensor (SeaWiFS)

106 We then used DeepBlue-SeaWiFS monthly mean AOD at 550 nm and AE products derived from SeaWiFS developed by NASA  
107 to study ocean color. SeaWiFS measures the solar radiation reflected at the top of the atmosphere in the wavelengths 412 nm,  
108 443 nm, 490 nm, 510 nm, 555 nm, 670 nm, 765 nm and 865 nm. Satellite measurements carried out between October 1997  
109 and December 2010 (Jamet et al., 2004; Hsu et al., 2012) have a value of signal-to-noise and uncertainty of 2%-3% for the  
110 different spectral bands (for details see (Eplee et al., 2007; Franz et al., 2007; Eplee Jr et al., 2011)). In this paper, we use the  
111 Level 3 version 4 products (Bettenhausen and Team, 2013) for years 2005 to 2010. The SeaWiFS AOD provided at 550 nm is  
112 available both over the land and over the ocean (Hsu et al., 2004; Sayer et al., 2012). The products used here are land-ocean es-  
113 timates generated and made available to the scientific community by NASA (Wang et al., 2000). Regarding the contribution of  
114 the aerosols types in the AOD, the studies of Dubovik et al. (2002); Schepanski et al. (2009b) or Tegen et al. (2013) suggested  
115 that the coarse mode fraction of mineral dust dominates the atmospheric mixture when AE values, associated with AOD values  
116 greater than or equal to 0.3, are below 0.7. Here, we consider aerosols optical thickness larger than 0.2 when the Ångström  
117 Exponent is lower than 0.7 (figure 4) to monitor the evolution of coarse (upper and lower bounds respectively) and fine (lower  
118 and upper bounds) modes of mineral aerosols.

119

### 120 **2.3 Ozone Monitoring Instrument (OMI)**

121 OMI is a passive sensor on board the Aura satellite launched on 15 July 2004 by NASA's EOS Aura space-craft which released  
122 its first observations in October 2004. Like all satellites in the A-Train constellation, OMI scans the entire Earth in 14 to 15  
123 orbits with a nadir ground pixel spatial resolution of  $13 \times 24 \text{ km}^2$  (Jethva et al., 2014). In addition to the ozone content in the  
124 atmosphere OMI provides information on aerosols, clouds, gases ( $\text{NO}_2$ ,  $\text{SO}_2$ ,  $\text{HCHO}$ ,  $\text{BrO}$ , and  $\text{OCIO}$ ) and irradiance in the ul-  
125 traviolet (Levelt et al., 2006). We use Aura/OMI SSA at 500 nm taken from <https://ozoneaq.gsfc.nasa.gov/data/lance-browse/>  
126 the OMAERUV Level 3 Collection 003 aerosol product processed in March 2012 with a spatial resolution of  $1^\circ \times 1^\circ$  to quantify  
127 the scattering of the aerosol types with passive sensors. The OMAERUV algorithm assigns flag to each pixel which carries  
128 information on the quality of the retrieval (Jethva et al., 2014).

129 The SSA represents the ratio (ranging between 0 and 1) of scattering coefficient to extinction coefficient and provides infor-  
130 mation about the absorbing properties of the aerosols. SSA of 0.9 indicates that 90% of the total extinction of solar light is  
131 caused by scattering and 10% by absorption effects (Jethva et al., 2014). This parameter depends on the wavelength, size and  
132 the complex refractive index of particles (Léon et al., 2009). The closer this value is to one the more desert aerosols dominate  
133 (Johnson et al., 2008; Léon et al., 2009; Ialongo et al., 2010; Malavelle, 2011).

134 OMI data were interpolated on the grid of SeaWiFS data to superimpose the products (AOD and SSA).

### 135 **2.4 Cloud Aerosol Lidar and Infrared Pathfinder Satellite Observations (CALIPSO)**

136 The first polarization lidar in space so-called CALIPSO is a sun-synchronous satellite developed by NASA as part of the  
137 Earth System Science Pathfinder program (ESSP) and launched on April 28, 2006 (Winker et al., 2007; Hunt et al., 2009) in  
138 order to provide a global coverage of the vertical distribution of the properties of clouds and aerosols (Winker, 2003). The  
139 [CALIOP](#) lidar (Light Detection and Ranging) ~~Cloud-Aerosol Backscatter Lidar with Orthogonal Polarization (CALIOP)~~ on-  
140 board CALIPSO acquires vertical profiles of the atmosphere at 30 m resolution in the lower layers (from the two orthogonal  
141 components that result from depolarization of a signal backscattered laser at 532 nm and vertical profiles of a total laser at 1064  
142 nm signal backscattered at nadir). The final level-2 product is reduced to a uniform resolution calculated from averaging and/or  
143 interpolating different resolutions for generating intermediate products (Winker et al., 2006). We use the Vertical Feature Mask  
144 (VFM; stage 1 Version 3) for which the processing algorithm is described in CALIOP Algorithm Theoretical Basis, Part 3:  
145 Scene Algorithms Classification (Liu et al., 2005). VFM allows to separate aerosols from clouds but also the desert aerosols  
146 from other types of aerosols (Omar et al., 2009). This methodology of discrimination by CALIOP of aerosol types gives results  
147 close to another method of distinction between mineral dust made from inversions (SSA and AE) of AERONET level 2 prod-  
148 ucts (Mielonen et al., 2009). The mix of layers of desert aerosol and other types of aerosols (i.e. biomass burning) is very rare  
149 (Chou et al., 2008; Heese and Wiegner, 2008) in our region of interest. During the dry season, mineral aerosols are observed  
150 in the atmospheric surface layer ranging 0.5 to 1 km while the aerosol emitted through biomass burning are carried to higher  
151 levels up to 5 km altitude (Cavalieri et al., 2010). Nevertheless, classification errors are possible for low values of the Mineral  
152 Dust Occurrence Frequency (MDOF) and at frontal zones between layers of different substances (Adams et al., 2012). For this

153 reason we only consider here the values of MDOF above 10%. Our method for determining the mineral dust by a calculation  
154 of the MDOF is equivalent to [\(Adams et al., 2012\)](#) expressed by the following [Adams et al. \(2012\)](#) and follows the equation:  
155

$$156 \quad p(x, y, z) = \frac{\sum_{n=0}^N p(x+n, y, z)}{\sum_{n=0}^N s(x+n, y, z)} \quad \forall \quad x, y, z \quad (1)$$

157

158

159 where  $p$  is the [probability-frequency](#) of occurrence of dust at a grid point,  $s$  the total number of valid satellite passing the  
160 same grid point and  $N$  the total number of grid points. [The Occurrences in the longitude \(x\) are summed and normalized by](#)  
161 [the total valid satellite passes in a given longitudinal range \(35°W-20°E\)](#). Data were gridded with a near-uniform horizontal  
162 resolution of  $0.5^\circ \times 0.5^\circ$  and a vertical resolution of 30 m for 290 vertical levels between 0.5 and 8.2 km above sea level. The  
163 CALIOP lidar on CALIPSO (also in the A-train) has a 90 m instantaneous footprint which is smeared to 333 m in the along  
164 track direction by orbital motion over the lidar pulse duration. All satellites of the A-train constellation, such as CALIPSO, fly  
165 in a sun-synchronous orbit with a 16 days coverage cycle consisting of 233 orbits separated by 1.54 degrees longitude or about  
166 172 km at the equator. Each satellite completes 14.55 orbits per day with a separation of 24.7 degrees longitude between each  
167 successive orbit at the equator. These CALIPSO orbits are controlled to cover the same ground with cross-track errors of less  
168 than  $\pm 10$  km (Winker et al., 2007). This drastically reduces the spatial coverage of the satellite. Consequently, we use a mesh  
169 of  $0.5^\circ$  longitude to cover the area between  $10^\circ\text{W}$ - $24^\circ\text{W}$  and  $12^\circ\text{N}$ - $21^\circ\text{N}$ . The choice of this band of latitude is driven by one  
170 of the objectives of the paper which is to study the transition of aerosol distribution between the continent and the ocean. Dust  
171 occurrences are averaged over latitudes  $12^\circ\text{N}$  to  $21^\circ\text{N}$  and are then smoothed over 30 points longitudinal running mean and 50  
172 points vertical running mean.

## 173 3 Results

### 174 3.1 Horizontal dust distribution

175 SeaWiFS AOD (estimated at wavelength 550 nm) represents an average value of the optical Depth of the atmosphere. It has first  
176 been compared to the monthly AOD given by AERONET photometers (given at the wavelength 675 nm [and interpolated at 550](#)  
177 [nm](#)) by calculating the correlation between the two measurements at different selected stations (Fig. 1). Our choice focused on  
178 the stations Banizoumbou ( $2.665^\circ\text{E}$ - $13.541^\circ\text{N}$ ), Agoufou ( $1.479^\circ\text{W}$ - $15.345^\circ\text{N}$ ), M'bour ( $16.959^\circ\text{W}$ - $14.394^\circ\text{N}$ ) and Capo Verde  
179 ( $22.935^\circ\text{W}$ - $16.733^\circ\text{N}$ ) to assess the quality of satellite information obtained across the land-ocean continuum. A very good  
180 correlation is calculated between SeaWiFS and in-situ measurement given by the photometer at Banizoumbou ( $R=0.950.97$ ;  
181 Fig. 1a). The photometer Cimel at Agoufou (Mali) also shows a very good correlation with SeaWiFS ( $R=0.920.87$ ; Fig. 1b).



182 The correlation between the two measures is equal to 0.81 at the shore in M'bour (Fig. 1c). It is close to the one in Capo Verde  
183 ( $R=0.83$ ; Fig. 1d). All these correlation values of AOD are significant at 95% using a student statistical test. The regression  
184 for M'bour site is not as good as for the other sites. This site is located at the shore at the interface between land and sea and  
185 the satellite algorithm retrieval is not the same over the land and over the ocean. We also studied the structure of the cloud of  
186 points between the two datasets to assess the quality of the satellite measurements as a function of the aerosol concentration.  
187 The regression line obtained by the least squares method shows a linear relationship between satellite and in-situ monthly mean  
188 measurements of AOD at the selected stations.

189 The horizontal transport of desert aerosols can be followed by considering the key and complementary parameters that distin-  
190 guish them. To better characterize the ~~desertie~~ desert aerosols, we combined AOD (SeaWiFS) with SSA (OMI) to specify the  
191 contribution of the latter compared to other types of aerosols in the atmosphere. A threshold of 0.90 in monthly averaged SSA  
192 is used to define regions dominated by desert aerosols. This value is chosen in agreement with the threshold value given in  
193 previous studies (Léon et al., 2009; Malavelle, 2011; Jethva et al., 2014). This method allowed us to define the Sahelo-Saharan  
194 region as the one which is the most influenced by dust plumes composed of desert aerosols throughout the year (between 12°N  
195 and 21°N; Fig. 3).

196 The comparison of the daily SSA of Aura/OMI versus AERONET is achieved to validate satellite SSA which provides a better  
197 spatio-temporal coverage of our region of interest. OMI SSA retrievals are taken between ~~10 and 15 am~~, 10am and 3pm time  
198 range which cover AERONET measurements. As emphasized by Jethva et al. (2014), this comparison is done at the original  
199 wavelengths of each independent measurement (388 nm for OMI and ~~438-440~~ nm for AERONET) in order to avoid uncertain-  
200 ties induced by the interpolation at other wavelengths. Good correlations are retrieved between the two datasets at the different  
201 ground stations in West Africa for the period 2005-2010 within root mean square (RMS) difference of 0.03 in the selected  
202 region (Fig. 2). Globally, the OMAERUV SSA is well correlated with ground measurements. The correlation at all selected  
203 sites for this study is significant. The agreement between the two inversions is better over the continent (Banizoumbou station,  
204  $r=0.47$  and Agoufou station:  $r=0.50$ ) and at the shore of West Africa (M'bour station:  $r=0.66$ ) ~~and than~~ over the ocean (Capo  
205 Verde station:  $r=0.30$ ) ~~than over the~~. The discrepancy between the AERONET SSA retrievals over continent (Banizoumbou  
206 ~~station,  $r=0.47$  and Agoufou station:  $r=0.50$ ) and Agoufou) and at the shore of West Africa (M'bour) was already found by~~  
207 (Johnson and Osborne, 2011) during GERBILS campaign over West Africa. These authors suggested that a lack of sampling  
208 may affect the results. Their results are in agreement with our results which show 449 retrievals in Banizoumbou against 178  
209 retrievals in M'bour site.

210 Figure 3 shows a seasonal distribution of the AOD which superposed onto SSA in West Africa region. Both, large AOD  
211 and strong SSA indicate that mineral dust is the dominant component in the aerosol in the atmosphere. In winter, the main  
212 dust source in West Africa, Bodélé depression, is showed in figure. 3a with AOD larger than 0.5 and SSA larger than 0.9  
213 around (17N-18E). This most persistent dust hot spot is activated along the year and provides a maximum dust emission  
214 in spring (Figure 3b), in agreement with Engelstaedter and Washington (2007) . In summer, the intense surface heating from  
215 solar radiation (Heat Low) induces the development of a near-surface thermal low pressure system over northern Mali, southern  
216 Algeria, and eastern Mauritania (Lavaysse et al., 2009; Messenger et al., 2010) and controls the dry convective processes which

217 contribute to about 35% of the global dust budget (Engelstaedter and Washington, 2007) . Over Northwestward Sahara region  
218 (Fig. 3c), the AOD is larger than 0.5 and SSA is stronger than 0.9, both variables indicate together the most hot spot mineral  
219 dust source in West Africa in summer which already showed by Engelstaedter and Washington (2007) .

220 Figure 3 and Figure 4 show that horizontal monthly average of AOD is stronger above the continent than over the ocean  
221 throughout the year. The weakest AOD is given for winter months (DJF for December-January-February) with a mean value  
222 of  $0.33 \pm 0.07$  (standard deviation). At this season, the SSA values are higher in the northeast tropical Atlantic than on the  
223 West African continent with a SSA maximum reaching 0.95. This indicates a stronger contribution of dust over the ocean  
224 than over the continent in the latitude range  $12^{\circ}\text{N}$ - $21^{\circ}\text{N}$ . Note that sources of dust aerosols are also indicated by high SSA  
225 values north of  $21^{\circ}\text{N}$ . The air masses advection in the lower atmosphere (925 hPa) follows a NorthEast-SouthWest direction in  
226 winter (figure 6a), dust coming from the NorthWest of Mauritania is partially seen over the continent (in AOD and SSA) and  
227 its main signature should be seen over the ocean. In spring (MAM for March-April-May), the increase of the monthly mean  
228 AOD compared to winter is indicated by a stronger mean value ( $0.50 \pm 0.08$ ). The mean optical depth indicates that the dust  
229 sources are becoming more active with an atmosphere more charged than in winter. The coarse mode dominates in the mixed  
230 atmosphere boundary layer over the continent with lower values of AE less than 0.7 (not shown). Nevertheless, the reflectance  
231 properties of aerosols (given by the SSA) is higher over the ocean than over the continent and vary weakly compared to winter.  
232 In summer (JJA for June-July-August), the maximum mean AOD is  $0.52 \pm 0.05$ . AOD values are associated with higher SSA  
233 above 0.96. It indicates that aerosols are clearly dominated by desert dust in boreal summer. At this season, ~~the largest dust~~  
234 ~~particules are mobilized and raised above the continent~~ important quantity of dust can be lifted up and vertically transported in the  
235 upper atmosphere by convective systems (e.g., ?, Fig. 4c) and near-surface convergence (Engelstaedter and Washington, 2007) .  
236 In autumn (SON for September-October-November), the monthly mean AOD is  $0.34 \pm 0.05$ . AOD is decreased compared to  
237 spring but the SSA values are much higher than in spring despite the fact that uplift occurrences are larger in spring than in fall  
238 in west Africa (Marticorena et al., 2010; Diokhane et al., 2016).

239 Changes of AOD and SSA are seen at the transition between the continent and the ocean (Fig. 4). Understanding these changes  
240 requires a thorough analysis of the vertical distribution of dust during transportation from east to west in North Africa.

### 241 **3.2 Vertical dust distribution**

242 The vertical distribution of desert aerosol indicates a strong presence of dust concentrations between the surface and 6 km in  
243 agreement with the results of Léon et al. (2009) who studied the vertical distribution of dust in the North-East Tropical Atlantic  
244 (Fig. 5).

245 In DJF, desert aerosols are mainly concentrated in the atmospheric boundary layer (ABL) between the surface and 2 km  
246 (Fig. 5a) both over the continent and the ocean. At this season, we also noted a homogeneous dust aerosol transition between  
247 Western Africa and the Eastern part of the Atlantic Ocean.

248 In MAM, there is an elevation of the SAL with a maximum altitude of 5 km on the continent and between 4 and 5 km above  
249 the ocean (Fig. 5b). The MDOF over 50% above the continent shows that dust emissions are much greater than in winter. ~~ABL~~  
250 ~~develops~~ The ABL is developed vertically to reach ~~the level of the SAL~~ up to 5 km of altitude. It results in an atmospheric layer



251 well mixed between the surface and 5 km of altitude above the continent (10°W-15°W). Above the Ocean we see a detachment  
252 of the SAL from the ocean surface which occurs at the coast (around 18°W).  
253 JJA is the busiest season of the year in terms of dust rising in the northern hemisphere of Africa. It is characterized by the de-  
254 velopment of density currents that intensify the mobilization of terrigenous aerosols (e.g., Bou Karam et al., 2008; Schepanski  
255 et al., 2009b, Fig. 5c).  
256 Unlike DJF, we note a clear separation of the dust layer above the Eastern Atlantic Ocean where dusts are confined between 1  
257 and 6 km altitude.  
258 In SON, dust emissions decrease in intensity compared to JJA but the detachment from the surface of the ocean remains clear  
259 at the coast although less marked than in JJA (Fig. 5d). According to Adams et al. (2012), the heart of the SAL is located about  
260 5 km above sea level in SON, whereas Liu et al. (2012) shows a maximum altitude of 4 km.

## 261 4 Discussion

### 262 4.1 Seasonal variability

263 The desert aerosols in the band of latitude 12°N-21°N are mainly emitted in the Saharan and Sahelian regions. Emissions and  
264 transport processes are mainly controlled by meteorological variables (Brooks and Legrand, 2000; Joseph, 1999).  
265 ~~In the Sahara, the Schepanski et al. (2009b) found that over the Sahara~~ sources of dust emissions are less active in winter  
266 than during ~~the other seasons and the summer season. The southward migration of the ITCZ and the subsiding branch of the~~  
267 ~~Hadley cell over the dry convection can also prevents the deep~~ vertical distribution of aerosols ~~is not supported by a favorable~~  
268 ~~wind regime ascending particles in north Africa (Lavaysse et al., 2009)~~. The maximum altitude of this distribution is 3 km  
269 above the continent and 2 km at the West African coast in agreement with the studies of (Léon et al., 2009) and (Vuolo  
270 et al., 2009). Compared to other seasons, DJF show an important role played by the shallower atmospheric layers on the dust  
271 transported from source regions located in the Northwestern part of Mauritania and more generally in the West African coastal  
272 region (Fig. 6a).~~These West African emission zones participate actively to the transport of mineral aerosols in the near Atlantic~~  
273 ~~Ocean.~~This high occurrence is shown by the inter-seasonal variability derived from NCEP Reanalysis. Figure 6 highlights  
274 that the Northwest region of Mauritania has the highest standard deviation of horizontal wind intensity between 18°N-24°N  
275 and that wind is very intense in winter compared to the other seasons (Fig. 6a). Hence this region represents an important sand  
276 source in winter as mentioned by previous studies (Bertrand et al., 1979; Ozer, 2000; Tulet et al., 2008; Laurent et al., 2008;  
277 Mokhtari, 2012; Hourdin et al., 2015).~~During this period, the studies of Dubovik et al. (2002); Schepanski et al. (2009b) or~~  
278 ~~Tegen et al. (2013) suggested that the coarse mode fraction of mineral dust dominates the atmospheric mixture as AE values~~  
279 ~~are below 0.7 (not shown) and are associated with AOD values greater than or equal to 0.3. Here, we have considered thresholds~~  
280 ~~of 0.7 for AE and 0.2 for AOD to monitor the evolution of coarse (upper and lower bounds respectively) and fine (lower and~~  
281 ~~upper bounds) modes of mineral aerosols.~~  
282 Unlike winter, ~~summer dust emissions are more concentrated in~~ as shows in figure 5c, dust are concentrated between the higher  
283 layers of the ABL up to 6 km (Gamo, 1996), from one to 5-6 km (Gamo, 1996), in response to intense convective mechanisms

284 that are more common in the region at this season (Cuesta et al., 2009). Indeed, the summer solar heating drives the development  
285 of the Saharan boundary layer which reaches up to 6 km while the convergence of hot, dry air (Harmatan/Harmattan) from the  
286 Sahara ~~and fresh, with fresh~~ moist air (monsoon) from the ocean ~~causes the raising and maintenance of aerosol layers between~~  
287 ~~1 and 6 km at the thermal front area of the inter-tropical discontinuity (ITD) for which the northern edge is located around~~  
288 ~~16°N (Fig. 6e).~~ generates intense convective cells which are responsible for the suspension of large amounts of dust which will  
289 be distributed in the ABL. Transport is also growing between 3 and 4 km above the ocean with a MDOF greater than 70%,  
290 i.e. more than 30% higher than that observed in DJF. This sharp increase of MDOF from DJF to JJA is in agreement with the  
291 results of (Schepanski et al., 2009b) who estimated an increase of more than 20% of the activity of dust sources in summer  
292 compared to winter in West Africa in the observations of Meteosat Second Generation (MSG) Spinning Enhanced Visible and  
293 Infrared Imager (SEVIRI). In summer, atmospheric dynamics raise large dust particles that are ~~subject to the law of universal~~  
294 ~~gravitation of Newton, thus settle much faster on the continent~~ settling down much closer to the source regions than the rest of  
295 the year (Shao, 2000). However, their reflectivity of solar radiation becomes larger and reaches a maximum value indicated by  
296 a SSA of 0.97 (Fig. 4c).

297 In autumn, SSA values are comparable to spring values but these high values are not due to high reflectance of desert aerosols  
298 like in spring because the southern migration of the Inter-Tropical Convergence Zone (ITCZ) reduces the activity of convective  
299 systems and causes a reduction of dust emissions shown by a decreasing of the AOD (Fig. 4d). These high SSA values can be  
300 attributed to atmospheric conditions seen through the relative humidity which is much higher than in spring (Fig. 7d). Indeed,  
301 OMI measures the atmospheric properties of the aerosols which are known to be hygroscopic (Jethva et al., 2014).

## 302 4.2 Continent-Ocean transition

303 To better understand the factors responsible for the high variability of the vertical transition of desert aerosols from the con-  
304 tinent to the ocean, we placed ourselves at a coastal point (Dakar) to study the variation of meteorological variables and their  
305 potential influence on the distribution of aerosols. Seasonality of vertical distributions of winds, relative humidity and potential  
306 temperature from radiosounding conducted at the weather station (GOOY) of Dakar (at West African shore) are shown in  
307 Figure 7.

308 In DJF, continental winds are very strong at the surface with a maximum of 22 m/s at 500 m (Fig. 7a). The north-east direction  
309 of the winds in the first thousand meters explains the homogeneity of the vertical distribution of dust from the continent towards  
310 the ocean. This north-east wind applies to all West Africa at the surface (Fig 6a). Their intensity also explains the strong values  
311 of MDOF (up to 50%) observed by CALIOP in wintertime above the continent. Between 1 and 2 km height, winds weaken and  
312 change direction (south to south-east) while MDOF observed by satellite decreases (Fig. 5a). Between 2 and 5 km height, the  
313 winds turn to the southwest and west. These dust-depleted air masses of oceanic origin are wetter than from the land, and limit  
314 the development of the ABL. The air masses of continental origin are located between the surface and 2000 m height (Fig. 7a).  
315 In Figure. 7a, the relative humidity is around 20% (between 500 and 2000 m) and it corresponds to a very dry air mass of  
316 Saharan origin. Between 2 and 5 km the potential temperature indicates a stable atmospheric layer. This season is associated  
317 with an intermediate AOD value which decreases from 15°E to 10°W. SSA reflects mineral dust properties across its westward

318 [transportation \(>0.9\) but is higher by 0.2 over the ocean than the continent. We believe it could reflect the transport of dust](#)  
319 [emitted along the coastline which is only partly taken into account in dust properties derived from the continent.](#)

320 Compared to the DJF situation, MAM surface winds (Fig. 7b) are intensifying to 25 m/s at 500 m height and are from the  
321 east. They are associated with MDOF above 50% in the ABL around 14°W. [Surface winds \(Fig 6b\) shows the near-surface](#)  
322 [convergence of northward and southward flows along 16°N which is associated with a well-mixed distribution of dust in the](#)  
323 [first 5 km of the atmosphere \(Fig 5b\) and higher AOD values than in winter \(Fig 4\).](#) There is an inversion of easterly winds  
324 between 1 and 3 km and a second southerly wind peak (15 m/s) appears between 3 and 4 km. It corresponds to the dust layer  
325 (SAL) detected by CALIOP. The vertical profile of potential temperature indicates a stable thick layer, well mixed between the  
326 surface and 3 km (Fig. 7b). Beyond this altitude there is a stable stratification of the atmosphere indicated also by the potential  
327 temperature. Between 3 and 5 km height, the air masses coming from the South to the South-Southwest are also of oceanic  
328 origin and their interaction with a more consistent amount of dust than in winter could explain the better marked transition be-  
329 tween the ocean and the continent in terms of SSA (increase) and AOD (decrease) for this season (Fig. 4b). Indeed, in general,  
330 increasing the relative humidity is likely to increase the SSA and size hygroscopic aerosols with dry to wet passage inducing a  
331 larger diameter even when humidity is below the saturation level (Hervo, 2013; Howell et al., 2006).

332 In JJA, surface winds (0-1 km) decrease and are from the West to the Southwest (West African Monsoon) (Fig. 7c). This  
333 corresponds to lower values of MDOF (Fig. 5c) but to relative humidity values well above DJF or MAM (Fig. 7). Reid et al.  
334 (2002) presented a conceptual model of Saharan dust transport in the middle troposphere describing an evolution of relative  
335 humidity profile in agreement with the observations made in Dakar. These authors describe a moistening of the surface layers  
336 due to monsoon flow which penetrates up to 1.5 km above this layer. [Figure 6c shows deep intrusion of air masses coming](#)  
337 [from the Gulf of Guinea which brings humidity into the continent. The dry convection taking place over the continent favors](#)  
338 [the vertical transport of dust to high altitudes \(Engelstaedter and Washington, 2007\).](#)

339 Between 2 and 6 km, winds are from the East and above 15 m/s. These wind velocity maxima reach 25 m/s in the range 3.5-5  
340 km and are associated to the African Easterly Jet (AEJ) (Wu et al., 2009; Lafore et al., 2011). The co-localization of the AEJ  
341 and the SAL between 2 and 5 km height (Fig. 5c and Fig. 7c) causes the westward SAL transport by AEJ in summer (Karyam-  
342 pudi et al., 1999). These strong winds correspond to the layer of dust detected by satellite at this altitude (Fig. 5c). Above the  
343 continent, the mesoscale features associated with the convergence between Harmattan and the West African Monsoon at the  
344 ITCZ cause strong updrafts that allow lifting and transport of dust particles throughout the air column (Tulet et al., 2008). The  
345 dynamics of the monsoon described by the conceptual scheme of mechanisms controlling the dust vertical redistribution in  
346 Cuesta et al. (2009) explain the wide occurrence of dust found between 2 and 5 km rather than at the surface. During transport  
347 from North Africa to the Atlantic Ocean, very large amounts of coarse dust (Fig. 4c) are deposited along the path with a rapid  
348 change in the size distribution of aerosols near the west African coast (Ryder et al., 2013). [The changes of the aerosol size and](#)  
349 [properties will impact the climate system \(Huneus et al., 2011; Mahowald et al., 2014\).](#) [McConnell et al. \(2008\) suggested](#)  
350 [that the variation in the aerosol profiles over the ocean have an impact on the radiative effect, a statement confirmed by](#)  
351 [Highwood et al. \(2003\) who showed that the radiative effect of mineral dust is correlated with the altitude of the dust layer.](#)

352 The signing of the SAL is evidenced by relative dryness of the atmosphere (Dulac et al., 2001) between 1.5 and 5 km (Fig. 7c).

353 At this altitude, the vertical profile of potential temperature indicates Saharan origin of air masses with temperatures between  
354 35°C and 45°C (Carlson and Prospero, 1972). The wind direction (east) given in Figure 7c between 1.5 and 5 km altitude  
355 confirms the origin of the Saharan air masses. The presence of dust in the SAL causes both warming and drying of the atmo-  
356 sphere between 1.5 and 5 km and a cooling below this layer (Tulet et al., 2008).

357 In SON, winds are weak and from the East at the surface (Fig. 7e and 6d). Between 1 and 5 km, it is increasing but is  
358 less intense than in JJA between 3 and 5 km and it is associated with a decrease of the MDOF (Fig. 5d). The moisture profile  
359 in SON (Fig. 7d) is close to that of JJA, but has a more humid atmosphere in the layer between 1.5 and 5 km where maxi-  
360 mum relative humidity of the year occurs (60%; Fig. 7d). The analysis of the vertical distribution of thermodynamic variables  
361 like relative humidity, potential temperature and wind measured at the Dakar weather station shows that the thermodynamical  
362 conditions control the dust vertical distribution as well as the depth of the dust layer depending on the season. This analysis  
363 also explains the unintuitive differences between spring, when the low values of SSA are associated with a strong AOD, and  
364 autumn characterized by high values of SSA associated with ~~comparable AOD~~ low AOD values.

## 365 5 Conclusions

366 Studies of processes involved in the vertical distribution of aerosols at the transition between continent and ocean are very rare.  
367 Here, we took advantage of a weather station ideally located on the main pathway of desert aerosols from Northern Africa  
368 (Léon et al., 2009; Marticorena et al., 2010; Mortier et al., 2016) to explain the effect of meteorological variables on this transi-  
369 tion in a region of primary importance worldwide. The interaction of air masses of oceanic origin with dust aerosols are crucial  
370 for understanding their fate (e.g., Friese et al., 2016). This study constitutes the first attempt to relate the seasonal dynamic  
371 of the atmosphere and the vertical distribution of dust aerosol in this region and provides the first dynamical explanation of a  
372 counterintuitive deposition pattern over the Atlantic ocean. Indeed, it explains the role of the local atmospheric circulation in  
373 driving a higher AOD and dust content in summer over west Africa in phase with dust deposition in Barbades islands but in  
374 opposition with Cape Verde islands where deposition is more intense in winter (Chiapello et al., 1995).

375 We have studied the seasonal variability of the distribution of desert aerosols in West Africa (continental and oceanic) from their  
376 optical and physical properties. First of all we have been able to show a good estimate of physical properties (AOD and SSA)  
377 of aerosols by satellite when compared with AERONET ground measurements on the mainland, the coast and the ocean. Space  
378 observations then allowed us to show the predominant presence of Saharan dust in the atmosphere north of 12°N throughout  
379 the year and an additional significant contribution of sandy sources from the Mauritanian coast in winter. The MDOF indicates  
380 a change in the vertical distribution of dust at the transition between the continent and the ocean, the largest differences occur-  
381 ring in spring and summer seasons. In DJF, the ABL is shallow (~ 1km) and strong winds from North-East transport the dust  
382 in a dry atmosphere from the continent to the ocean continuously. This surface layer is superimposed by a stable atmospheric  
383 layer which inhibits the vertical development of this surface layer rich in dust aerosols. The decrease from east to west of the  
384 AOD requires material deposition during the transit. ~~In summer, convection~~ In summer dry convection located north of 10°N  
385 and associated with structures that develop at the ~~ITCZ distribute dust over~~ Inter-Tropical discontinuity (ITD) distribute dust

386 [up to 6 km height and create a thicker AOD. Above 6 km altitude over the Saharan-sahel areas, the vertical distribution of dust](#)  
387 [is bocked by the strong subsiding branch of the Hadley cell \(Lavaysse et al., 2009\)](#). In the lower layers, the westward oceanic  
388 moistly entries which are opposite to the higher eastward winds generate very different distributions above the continent or the  
389 ocean. On the mainland, the dust is dominated by coarse mode and have a homogeneous vertical distribution while above the  
390 ocean, lower layers are poor in dust and are superimposed by the SAL which is highly enriched. The SSA remains constant at  
391 this transition. MAM and SON represent transition periods, ~~MAM~~. [For the vertical dust distribution, MAM is](#) being closer to  
392 the summer situation.

393 Future modeling experiments should bring further insights into ocean-atmosphere processes involved in explaining this transi-  
394 tion and the dust deposition along this pathway. It also seems that a more tailored approach to ocean-atmosphere interactions  
395 including higher frequencies of variability and notably the diurnal cycle is needed to make more apparent the role of local  
396 circulation on the vertical distribution of aerosols in coastal areas.

397 *Acknowledgements.* We would like to thank the IRD-BMBF AWA project and the international joint laboratory ECLAIRS for supporting  
398 and promoting our research activities. We thank the Institute of Research for Development for funding this PhD. We also thank ICARE for  
399 the online availability of the CALIPSO aerosol products at <http://www.icare.univ-lille1.fr/archive>. NCEP Reanalysis data were found online  
400 by the <http://www.esrl.noaa.gov/psd/data/gridded/data.ncep.reanalysis.pressure.html>, and the PIs and NASA for online AERONET data set  
401 which can be obtained from <http://aeronet.gsfc.nasa.gov/>. OMI aerosol products were downloaded at [http://disc.gsfc.nasa.gov/gesNews/  
402 giovanni\\_3\\_end\\_of\\_service?instance\\_id=omil2g&selectedMap=Blue%2520Marble&](http://disc.gsfc.nasa.gov/gesNews/giovanni_3_end_of_service?instance_id=omil2g&selectedMap=Blue%2520Marble&). We are finally very grateful to B. Marticorena and I.  
403 Chiapello for very fruitful discussions.

## 404 References

- 405 Adams, A. M., Prospero, J. M., and Zhang, C.: CALIPSO-derived three-dimensional structure of aerosol over the Atlantic Basin and adjacent  
406 continents, *Journal of Climate*, 25, 6862–6879, 2012.
- 407 [Alizadeh-Choobari, O., Sturman, A., and Zawar-Reza, P.: A global satellite view of the seasonal distribution of mineral dust and its correlation  
408 with atmospheric circulation, \*Dynamics of Atmospheres and Oceans\*, 68, 20–34, 2014.](#)
- 409 Andreae, M. O. et al.: Raising dust in the greenhouse, *Nature*, 380, 389–390, 1996.
- 410 [Ansmann, A., Bösenberg, J., Chaikovsky, A., Comerón, A., Eckhardt, S., Eixmann, R., Freudenthaler, V., Ginoux, P., Komguem, L., Linné,  
411 H., et al.: Long-range transport of Saharan dust to northern Europe: The 11–16 October 2001 outbreak observed with EARLINET, \*Journal  
412 of Geophysical Research: Atmospheres\*, 108, 2003.](#)
- 413 [Ansmann, A., Baars, H., Tesche, M., Müller, D., Althausen, D., Engelmann, R., Pauliquevis, T., and Artaxo, P.: Dust and smoke transport  
414 from Africa to South America: Lidar profiling over Cape Verde and the Amazon rainforest, \*Geophysical Research Letters\*, 36, 2009.](#)
- 415 Arístegui, J., Barton, E. D., Álvarez-Salgado, X. A., Santos, A. M. P., Figueiras, F. G., Kifani, S., Hernández-León, S., Mason, E., Machú,  
416 E., and Demarcq, H.: Sub-regional ecosystem variability in the Canary Current upwelling, *Progress in Oceanography*, 83, 33–48, 2009.
- 417 Baker, A., Kelly, S., Biswas, K., Witt, M., and Jickells, T.: Atmospheric deposition of nutrients to the Atlantic Ocean, *Geophysical Research  
418 Letters*, 30, 2003.
- 419 Ben-Ami, Y., Koren, I., and Altaratz, O.: Patterns of North African dust transport over the Atlantic: winter vs. summer, based on CALIPSO  
420 first year data, *Atmospheric Chemistry and Physics*, 9, 7867–7875, 2009.
- 421 Ben-Ami, Y., Koren, I., Rudich, Y., Artaxo, P., Martin, S., and Andreae, M.: Transport of North African dust from the Bodélé depression to  
422 the Amazon Basin: a case study, *Atmospheric Chemistry and Physics*, 10, 7533–7544, 2010.
- 423 [Bergametti, G., DUTOT, A.-L., BUAT-MÉNARD, P., Losno, R., and Remoudaki, E.: Seasonal variability of the elemental composition of  
424 atmospheric aerosol particles over the northwestern Mediterranean, \*Tellus B\*, 41, 353–361, 1989.](#)
- 425 Bertrand, J., Cerf, A., and Domergue, J.: Repartition in space and time of dust haze south of the Sahara, *The Long-Range Transport of  
426 Pollutants and its Relation to Gen. Circulation Including Stratospheric/Tropospheric Exchange Processes* p 409-415(SEE N 80-26888  
427 17-45), 1979.
- 428 Bettenhausen, C. and Team, G. D. M.: Consistent Long-Term Aerosol Data Records over Land and Ocean from SeaWiFS, in: *Goddard Space  
429 Flight Center Greenbelt, Maryland*, pp. 1–19, <http://disc.sci.gsfc.nasa.gov/dust/documentation/README.DeepBlueSeaWiFS.pdf>, 2013.
- 430 Bou Karam, D., Flamant, C., Knippertz, P., Reitebuch, O., Pelon, J., Chong, M., and Dabas, A.: Dust emissions over the Sahel associated with  
431 the West African monsoon intertropical discontinuity region: A representative case-study, *Quarterly Journal of the Royal Meteorological  
432 Society*, 134, 621–634, 2008.
- 433 Braun, S. A.: Reevaluating the role of the Saharan air layer in Atlantic tropical cyclogenesis and evolution, *Monthly Weather Review*, 138,  
434 2007–2037, 2010.
- 435 Brooks, N. and Legrand, M.: Dust variability over northern Africa and rainfall in the Sahel, in: *Linking climate change to land surface  
436 change*, pp. 1–25, Springer, 2000.
- 437 Cakmur, R. V., Miller, R. L., and Tegen, I.: A comparison of seasonal and interannual variability of soil dust aerosols over the Atlantic Ocean  
438 as inferred by the TOMS AI and AVHRR AOT retrievals, *Journal of Geophysical Research: Atmospheres*, 106, 18 287–18 303, 2001.
- 439 Carlson, T. N. and Prospero, J. M.: The large-scale movement of Saharan air outbreaks over the northern equatorial Atlantic, *Journal of  
440 applied meteorology*, 11, 283–297, 1972.



441 Cavalieri, O., Cairo, F., Fierli, F., Donfrancesco, G. D., Snels, M., Viterbini, M., Cardillo, F., Chatenet, B., Formenti, P., Marticorena, B.,  
442 et al.: Variability of aerosol vertical distribution in the Sahel, *Atmospheric Chemistry and Physics*, 10, 12 005–12 023, 2010.

443 Chiapello, I. and Moulin, C.: TOMS and METEOSAT satellite records of the variability of Saharan dust transport over the Atlantic during  
444 the last two decades (1979–1997), *Geophysical Research Letters*, 29, 2002.

445 Chiapello, I., Bergametti, G., Gomes, L., Chatenet, B., Dulac, F., Pimenta, J., and Santos Soares, E.: An additional low layer transport of  
446 Sahelian and Saharan dust over the north-eastern tropical Atlantic, *Geophysical Research Letters*, 22, 3191–3194, 1995.

447 Chiapello, I., Prospero, J., Herman, J., and Hsu, N.: Detection of mineral dust over the North Atlantic Ocean and Africa with the Nimbus 7  
448 TOMS, *Journal of Geophysical Research: Atmospheres*, 104, 9277–9291, 1999.

449 Chou, C., Formenti, P., Maille, M., Ausset, P., Helas, G., Osborne, S., and Harrison, M.: Size distribution, shape and composition of dust  
450 aerosols collected during the AMMA SOP0 field campaign in the northeast of Niger, January 2006, *J. Geophys. Res.*, 113, D00C10, 2008.

451 Claquin, T., Schulz, M., and Balkanski, Y.: Modeling the mineralogy of atmospheric dust sources, *Journal of Geophysical Research: Atmo-*  
452 *spheres*, 104, 22 243–22 256, 1999.

453 Cuesta, J., Marsham, J. H., Parker, D. J., and Flamant, C.: Dynamical mechanisms controlling the vertical redistribution of dust and the  
454 thermodynamic structure of the West Saharan atmospheric boundary layer during summer, *Atmospheric Science Letters*, 10, 34–42, 2009.

455 Diokhane, A. M., Jenkins, G. S., Manga, N., Drame, M. S., and Mbodji, B.: Linkages between observed, modeled Saharan dust loading and  
456 meningitis in Senegal during 2012 and 2013, *International journal of biometeorology*, 60, 557–575, 2016.

457 Dubovik, O., Smirnov, A., Holben, B., King, M., Kaufman, Y., Eck, T., and Slutsker, I.: Accuracy assessments of aerosol optical properties re-  
458 trieved from Aerosol Robotic Network (AERONET) Sun and sky radiance measurements, *Journal of Geophysical Research: Atmospheres*,  
459 105, 9791–9806, 2000.

460 Dubovik, O., Holben, B., Eck, T. F., Smirnov, A., Kaufman, Y. J., King, M. D., Tanré, D., and Slutsker, I.: Variability of absorption and  
461 optical properties of key aerosol types observed in worldwide locations, *Journal of the atmospheric sciences*, 59, 590–608, 2002.

462 Duce, R. A. and Tindale, N. W.: Atmospheric transport of iron and its deposition in the ocean, *Limnology and Oceanography*, 36, 1715–1726,  
463 1991.

464 Dulac, F., Chazette, P., Gomes, L., Chatenet, B., Berger, H., and Dos Santos, J. V.: A method for aerosol profiling in the lower troposphere  
465 with coupled scatter and meteorological rawinsondes and first data from the tropical Atlantic off Sahara, *Journal of aerosol science*, 32,  
466 1069–1086, 2001.

467 Dunion, J. P. and Marron, C. S.: A reexamination of the Jordan mean tropical sounding based on awareness of the Saharan air layer: Results  
468 from 2002, *Journal of Climate*, 21, 5242–5253, 2008.

469 [Engelstaedter, S. and Washington, R.: Atmospheric controls on the annual cycle of North African dust, \*Journal of Geophysical Research: Atmospheres\*, 112, 2007.](#)

470

471 Engelstaedter, S., Tegen, I., and Washington, R.: North African dust emissions and transport, *Earth-Science Reviews*, 79, 73–100, 2006.

472 Eplee, R. E., Patt, F. S., Barnes, R. A., and McClain, C. R.: SeaWiFS long-term solar diffuser reflectance and sensor noise analyses, *Applied*  
473 *optics*, 46, 762–773, 2007.

474 Eplee Jr, R. E., Sun, J.-Q., Meister, G., Patt, F. S., Xiong, X., and McClain, C. R.: Cross calibration of SeaWiFS and MODIS using on-orbit  
475 observations of the Moon, *Applied Optics*, 50, 120–133, 2011.

476 [Formenti, P., Andreae, M., Lange, L., Roberts, G., Cafmeyer, J., Rajta, I., Maenhaut, W., Holben, B., Artaxo, P., and Lelieveld, J.: Saharan dust in Brazil and Suriname during the Large-Scale Biosphere-Atmosphere Experiment in Amazonia \(LBA\)-Cooperative LBA Regional Experiment \(CLAIRE\) in March 1998, \*Journal of Geophysical Research: Atmospheres\*, 106, 14 919–14 934, 2001.](#)

477

478

479 Formenti, P., Rajot, J. L., Desboeufs, K., Caquineau, S., Chevaillier, S., Nava, S., Gaudichet, A., Journet, E., Triquet, S., Alfaro, S., et al.:  
480 Regional variability of the composition of mineral dust from western Africa: Results from the AMMA SOP0/DABEX and DODO field  
481 campaigns, *Journal of Geophysical Research: Atmospheres*, 113, 2008.

482 Franz, B. A., Bailey, S. W., Werdell, P. J., and McClain, C. R.: Sensor-independent approach to the vicarious calibration of satellite ocean  
483 color radiometry, *Applied optics*, 46, 5068–5082, 2007.

484 Friese, C. A., van der Does, M., Merkel, U., Iversen, M. H., Fischer, G., and Stuut, J.-B. W.: Environmental factors controlling the seasonal  
485 variability in particle size distribution of modern Saharan dust deposited off Cape Blanc, *Aeolian Research*, 22, 165–179, 2016.

486 Gamo, M.: Thickness of the dry convection and large-scale subsidence above deserts, *Boundary-Layer Meteorology*, 79, 265–278, 1996.

487 [Ganor, E. and Mamane, Y.: Transport of Saharan dust across the eastern Mediterranean, \*Atmospheric Environment\* \(1967\), 16, 581–587, 1982.](#)

488

489 [Ganor, E., Osetinsky, I., Stupp, A., and Alpert, P.: Increasing trend of African dust, over 49 years, in the eastern Mediterranean, \*Journal of Geophysical research: atmospheres\*, 115, 2010.](#)

490

491 Generoso, S., Bey, I., Labonne, M., and Bréon, F.-M.: Aerosol vertical distribution in dust outflow over the Atlantic: Comparisons between  
492 GEOS-Chem and Cloud-aerosol Lidar and Infrared Pathfinder Satellite Observation (CALIPSO), *Journal of Geophysical Research: At-*  
493 *mospheres*, 113, 2008.

494 Griffin, D. W.: Atmospheric movement of microorganisms in clouds of desert dust and implications for human health, *Clinical microbiology*  
495 *reviews*, 20, 459–477, 2007.

496 Heese, B. and Wiegner, M.: Vertical aerosol profiles from Raman polarization lidar observations during the dry season AMMA field cam-  
497 paign, *Journal of Geophysical Research: Atmospheres*, 113, 2008.

498 Hervo, M.: Etude des propriétés optiques et radiatives des aérosols en atmosphère réelle: Impact de l'hygroscopicité, Ph.D. thesis, Université  
499 Blaise Pascal-Clermont-Ferrand II, 2013.

500 [Highwood, E. J., Haywood, J. M., Silverstone, M. D., Newman, S. M., and Taylor, J. P.: Radiative properties and direct effect of Saharan dust measured by the C-130 aircraft during Saharan Dust Experiment \(SHADE\): 2. Terrestrial spectrum, \*Journal of Geophysical Research: Atmospheres\*, 108, 2003.](#)

501

502

503 Holben, B., Tanre, D., Smirnov, A., Eck, T., Slutsker, I., Abuhassan, N., Newcomb, W., Schafer, J., Chatenet, B., Lavenu, F., et al.: An  
504 emerging ground-based aerosol climatology: Aerosol optical depth from AERONET, *Journal of Geophysical Research: Atmospheres*,  
505 106, 12 067–12 097, 2001.

506 Holben, B. N., Eck, T., Slutsker, I., Tanre, D., Buis, J., Setzer, A., Vermote, E., Reagan, J. A., Kaufman, Y., Nakajima, T., et al.:  
507 AERONET—A federated instrument network and data archive for aerosol characterization, *Remote sensing of environment*, 66, 1–16,  
508 1998.

509 Hourdin, F., Gueye, M., Diallo, B., Dufresne, J.-L., Escribano, J., Menut, L., Marticoréna, B., Siour, G., and Guichard, F.: Parameterization  
510 of convective transport in the boundary layer and its impact on the representation of the diurnal cycle of wind and dust emissions,  
511 *Atmospheric Chemistry and Physics*, 15, 6775–6788, 2015.

512 Howell, S., Clarke, A., Shinzuka, Y., Kapustin, V., McNaughton, C., Huebert, B., Doherty, S., and Anderson, T.: Influence of relative  
513 humidity upon pollution and dust during ACE-Asia: Size distributions and implications for optical properties, *Journal of Geophysical*  
514 *Research: Atmospheres*, 111, 2006.

515 Hsu, N., Gautam, R., Sayer, A., Bettenhausen, C., Li, C., Jeong, M., Tsay, S., and Holben, B.: Global and regional trends of aerosol optical  
516 depth over land and ocean using SeaWiFS measurements from 1997 to 2010, 2012.

517 Hsu, N. C., Tsay, S.-C., King, M. D., and Herman, J. R.: Aerosol properties over bright-reflecting source regions, *IEEE Transactions on*  
518 *Geoscience and Remote Sensing*, 42, 557–569, 2004.

519 [Huneus, N., Schulz, M., Balkanski, Y., Griesfeller, J., Prospero, J., Kinne, S., Bauer, S., Boucher, O., Chin, M., Dentener, F., et al.: Global](#)  
520 [dust model intercomparison in AeroCom phase I, \*Atmospheric Chemistry and Physics\*, 11, 2011.](#)

521 Hunt, W. H., Winker, D. M., Vaughan, M. A., Powell, K. A., Lucker, P. L., and Weimer, C.: CALIPSO lidar description and performance  
522 assessment, *Journal of Atmospheric and Oceanic Technology*, 26, 1214–1228, 2009.

523 ~~Husar, R.-B., Prospero, J. M., and Stowe, L. L.: Characterization of tropospheric aerosols over the oceans with the NOAA advanced very~~  
524 ~~high-resolution-radiometer-optical-thickness-operational-product, *Journal of Geophysical Research: Atmospheres*, 102, 16889–16909,~~  
525 ~~1997.~~

526 Ialongo, I., Buchard, V., Brogniez, C., Casale, G., and Siani, A.: Aerosol Single Scattering Albedo retrieval in the UV range: an application  
527 to OMI satellite validation, *Atmospheric Chemistry and Physics*, 10, 331–340, 2010.

528 [Israelevich, P., Ganor, E., Levin, Z., and Joseph, J.: Annual variations of physical properties of desert dust over Israel, \*Journal of Geophysical\*](#)  
529 [Research: Atmospheres, 108, 2003.](#)

530 Jamet, C., Moulin, C., and Thiria, S.: Monitoring aerosol optical properties over the Mediterranean from SeaWiFS images using a neural  
531 network inversion, *Geophysical Research Letters*, 31, 2004.

532 Jethva, H., Torres, O., and Ahn, C.: Global assessment of OMI aerosol single-scattering albedo using ground-based AERONET inversion,  
533 *Journal of Geophysical Research: Atmospheres*, 119, 9020–9040, 2014.

534 Jickells, T., An, Z., Andersen, K. K., Baker, A., Bergametti, G., Brooks, N., Cao, J., Boyd, P., Duce, R., Hunter, K., et al.: Global iron  
535 connections between desert dust, ocean biogeochemistry, and climate, *science*, 308, 67–71, 2005.

536 [Johnson, B. and Osborne, S.: Physical and optical properties of mineral dust aerosol measured by aircraft during the GERBILS campaign,](#)  
537 [Quarterly Journal of the Royal Meteorological Society, 137, 1117–1130, 2011.](#)

538 Johnson, B., Osborne, S., Haywood, J., and Harrison, M.: Aircraft measurements of biomass burning aerosol over West Africa during  
539 DABEX, *Journal of Geophysical Research: Atmospheres*, 113, 2008.

540 Joseph, M.: Long-term measurements of the transport of African mineral dust to the southeastern United States: Implications for regional air  
541 quality, 1999.

542 Karyampudi, V. M., Palm, S. P., Reagen, J. A., Fang, H., et al.: Validation of the Saharan dust plume conceptual model using lidar, Meteosat,  
543 and ECMWF data, *Bulletin of the American Meteorological Society*, 80, 1045, 1999.

544 Kaufman, Y., Koren, I., Remer, L., Tanré, D., Ginoux, P., and Fan, S.: Dust transport and deposition observed from the Terra-Moderate  
545 Resolution Imaging Spectroradiometer (MODIS) spacecraft over the Atlantic Ocean, *Journal of Geophysical Research: Atmospheres*,  
546 110, 2005.

547 Lafore, J.-P., Flamant, C., Guichard, F., Parker, D., Bouniol, D., Fink, A., Giraud, V., Gosset, M., Hall, N., Höller, H., et al.: Progress in  
548 understanding of weather systems in West Africa, *Atmospheric Science Letters*, 12, 7–12, 2011.

549 Laurent, B., Marticorena, B., Bergametti, G., Léon, J., and Mahowald, N.: Modeling mineral dust emissions from the Sahara desert using  
550 new surface properties and soil database, *Journal of Geophysical Research: Atmospheres*, 113, 2008.

551 [Lavaysse, C., Flamant, C., Janicot, S., Parker, D., Lafore, J.-P., Sultan, B., and Pelon, J.: Seasonal evolution of the West African heat low: a](#)  
552 [climatological perspective, \*Climate Dynamics\*, 33, 313–330, 2009.](#)

553 Léon, J.-F., Derimian, Y., Chiapello, I., Tanré, D., Podvin, T., Chatenet, B., Diallo, A., and Deroo, C.: Aerosol vertical distribution and optical  
554 properties over M’Bour (16.96 W; 14.39 N), Senegal from 2006 to 2008, *Atmospheric Chemistry and Physics*, 9, 9249–9261, 2009.

555 Levelt, P. F., van den Oord, G. H., Dobber, M. R., Malkki, A., Visser, H., de Vries, J., Stammes, P., Lundell, J. O., and Saari, H.: The ozone  
556 monitoring instrument, *IEEE Transactions on geoscience and remote sensing*, 44, 1093–1101, 2006.

557 Liu, D., Wang, Z., Liu, Z., Winker, D., and Trepte, C.: A height resolved global view of dust aerosols from the first year CALIPSO lidar  
558 measurements, *Journal of Geophysical Research: Atmospheres*, 113, 2008.

559 Liu, D., Wang, Y., Wang, Z., and Zhou, J.: The three-dimensional structure of transatlantic African dust transport: a new perspective from  
560 CALIPSO LIDAR measurements, *Advances in Meteorology*, 2012, 2012.

561 Liu, Z., Omar, A., Hu, Y., Vaughan, M., Winker, D., Poole, L., and Kovacs, T.: CALIOP algorithm theoretical basis document. Part 3: Scene  
562 classification algorithms, NASA-CNES document PC-SCI-203, 2005.

563 [Mahowald, N., Albani, S., Kok, J. F., Engelstaeder, S., Scanza, R., Ward, D. S., and Flanner, M. G.: The size distribution of desert dust  
564 aerosols and its impact on the Earth system, \*Aeolian Research\*, 15, 53–71, 2014.](#)

565 Mahowald, N. M., Engelstaedter, S., Luo, C., Sealy, A., Artaxo, P., Benitez-Nelson, C., Bonnet, S., Chen, Y., Chuang, P. Y., Cohen, D. D.,  
566 et al.: Atmospheric Iron Deposition: Global Distribution, Variability, and Human Perturbations\*, *Annual Review of Marine Science*, 1,  
567 245–278, 2009.

568 Malavelle, F.: Effets direct et semi-direct des aérosols en Afrique de l’ouest pendant la saison sèche, Ph.D. thesis, Université Paul Sabatier-  
569 Toulouse III, 2011.

570 Marticorena, B., Chatenet, B., Rajot, J.-L., Traoré, S., Coulibaly, M., Diallo, A., Koné, I., Maman, A., NDiaye, T., and Zakou, A.: Temporal  
571 variability of mineral dust concentrations over West Africa: analyses of a pluriannual monitoring from the AMMA Sahelian Dust Transect,  
572 *Atmospheric Chemistry and Physics*, 10, 8899–8915, 2010.

573 Martin, J. H.: Iron as a limiting factor in oceanic productivity, in: *Primary productivity and biogeochemical cycles in the sea*, pp. 123–137,  
574 Springer, 1992.

575 Martiny, N. and Chiapello, I.: Assessments for the impact of mineral dust on the meningitis incidence in West Africa, *Atmospheric Environ-  
576 ment*, 70, 245–253, 2013.

577 [McConnell, C., Highwood, E., Coe, H., Formenti, P., Anderson, B., Osborne, S., Nava, S., Desboeufs, K., Chen, G., and Harrison, M.:  
578 Seasonal variations of the physical and optical characteristics of Saharan dust: Results from the Dust Outflow and Deposition to the Ocean  
579 \(DODO\) experiment, \*Journal of Geophysical Research: Atmospheres\*, 113, 2008.](#)

580 [Messenger, C., Parker, D. J., Reitebuch, O., Agusti-Panareda, A., Taylor, C. M., and Cuesta, J.: Structure and dynamics of the Saharan  
581 atmospheric boundary layer during the West African monsoon onset: Observations and analyses from the research flights of 14 and 17  
582 July 2006, \*Quarterly Journal of the Royal Meteorological Society\*, 136, 107–124, 2010.](#)

583 Mielonen, T., Arola, A., Komppula, M., Kukkonen, J., Koskinen, J., de Leeuw, G., and Lehtinen, K.: Comparison of CALIOP level 2 aerosol  
584 subtypes to aerosol types derived from AERONET inversion data, *Geophysical Research Letters*, 36, 2009.

585 Mills, M. M., Ridame, C., Davey, M., La Roche, J., and Geider, R. J.: Iron and phosphorus co-limit nitrogen fixation in the eastern tropical  
586 North Atlantic, *Nature*, 429, 292–294, 2004.

587 Mokhtari, M.: Amélioration de la prise en compte des aérosols terrigènes dans les modèles atmosphériques à moyenne échelle, Ph.D. thesis,  
588 Université de Toulouse, Université Toulouse III-Paul Sabatier, 2012.

589 Mortier, A., Goloub, P., Derimian, Y., Tanré, D., Podvin, T., Blarel, L., Deroo, C., Marticorena, B., Diallo, A., and Ndiaye, T.: Climatology  
590 of aerosol properties and clear-sky shortwave radiative effects using Lidar and Sun photometer observations in the Dakar site, *Journal of  
591 Geophysical Research: Atmospheres*, 2016.

592 Moulin, C.: Transport atmosphérique des poussières africaines sur la Méditerranée et l'Atlantique: climatologie satellitale à partir des images  
593 Météosat VIS(1983-1994) et relations avec le climat, Ph.D. thesis, 1997.

594 Omar, A. H., Winker, D. M., Vaughan, M. A., Hu, Y., Trepte, C. R., Ferrare, R. A., Lee, K.-P., Hostetler, C. A., Kittaka, C., Rogers, R. R.,  
595 et al.: The CALIPSO automated aerosol classification and lidar ratio selection algorithm, *Journal of Atmospheric and Oceanic Technology*,  
596 26, 1994–2014, 2009.

597 Ozer, P.: Les lithométéores en région sahélienne: un indicateur climatique de la désertification, Ph.D. thesis, Université de Liège Faculté des  
598 sciences Liège Belgique, Liège, Belgique, 2000.

599 Petzold, A., Veira, A., Mund, S., Esselborn, M., Kiemle, C., Weinzierl, B., Hamburger, T., Ehret, G., Lieke, K., and Kandler, K.: Mixing of  
600 mineral dust with urban pollution aerosol over Dakar (Senegal): impact on dust physico-chemical and radiative properties, *Tellus B*, 63,  
601 619–634, 2011.

602 Prospero, J., Glaccum, R., and Nees, R.: Atmospheric transport of soil dust from Africa to South America, *Nature*, 289, 570–572, 1981.

603 Prospero, J. M., Blades, E., Mathison, G., and Naidu, R.: Interhemispheric transport of viable fungi and bacteria from Africa to the Caribbean  
604 with soil dust, *Aerobiologia*, 21, 1–19, 2005.

605 ~~Rajot, J.-L.: Wind-blown sediment mass budget of Sahelian village land units in Niger, *Bulletin de la Société Géologique de France*, 172,  
606 523–531, 2001.~~

607 Ramanathan, V., Crutzen, P., Kiehl, J., and Rosenfeld, D.: Aerosols, climate, and the hydrological cycle, *science*, 294, 2119–2124, 2001.

608 Reid, J. S., Westphal, D. L., Livingston, J. M., Savoie, D. L., Maring, H. B., Jonsson, H. H., Eleuterio, D. P., Kinney, J. E., and Reid, E. A.:  
609 Dust vertical distribution in the Caribbean during the Puerto Rico Dust Experiment, *Geophysical research letters*, 29, 2002.

610 Ridley, D., Heald, C., and Ford, B.: North African dust export and deposition: A satellite and model perspective, *Journal of Geophysical  
611 Research: Atmospheres*, 117, 2012.

612 Ryder, C., Highwood, E., Lai, T., Sodemann, H., and Marsham, J.: Impact of atmospheric transport on the evolution of microphysical and  
613 optical properties of Saharan dust, *Geophysical Research Letters*, 40, 2433–2438, 2013.

614 Sayer, A., Hsu, N., Bettenhausen, C., Ahmad, Z., Holben, B., Smirnov, A., Thomas, G., and Zhang, J.: SeaWiFS Ocean Aerosol Retrieval  
615 (SOAR): Algorithm, validation, and comparison with other data sets, *Journal of Geophysical Research: Atmospheres*, 117, 2012.

616 [Schepanski, K., Tegen, I., Laurent, B., Heinold, B., and Macke, A.: A new Saharan dust source activation frequency map derived from  
617 MSG-SEVIRI IR-channels, \*Geophysical Research Letters\*, 34, 2007.](#)

618 Schepanski, K., Tegen, I., and Macke, A.: Saharan dust transport and deposition towards the tropical northern Atlantic, *Atmos. Chem. Phys*,  
619 9, 1173–1189, 2009a.

620 Schepanski, K., Tegen, I., Todd, M., Heinold, B., Bönisch, G., Laurent, B., and Macke, A.: Meteorological processes forcing Saharan dust  
621 emission inferred from MSG-SEVIRI observations of subdaily dust source activation and numerical models, *Journal of Geophysical  
622 Research: Atmospheres*, 114, 2009b.

623 [Schepanski, K., Tegen, I., and Macke, A.: Comparison of satellite based observations of Saharan dust source areas, \*Remote Sensing of  
624 Environment\*, 123, 90–97, 2012.](#)

625 [Shao, Y.: \*Physics and modelling of wind erosion \(atmospheric and oceanographic sciences library\)\*, 2000.](#)

626 Slutsker, I. and Kinne, S.: Wavelength dependence of the optical depth of biomass burning, urban, and desert dust aerosols, *J Geophys Res*,  
627 104, 00 093–5, 1999.

628 Sokolik, I. N. and Toon, O. B.: Incorporation of mineralogical composition into models of the radiative properties of mineral aerosol from  
629 UV to IR wavelengths, *Journal of Geophysical Research*, 104, 9423–9444, 1999.

630 Solomon, S.: Climate change 2007-the physical science basis: Working group I contribution to the fourth assessment report of the IPCC,  
631 vol. 4, Cambridge University Press, 2007.

632 Stith, J., Ramanathan, V., Cooper, W., Roberts, G., DeMott, P., Carmichael, G., Hatch, C., Adhikary, B., Twohy, C., Rogers, D., et al.: An  
633 overview of aircraft observations from the Pacific Dust Experiment campaign, *Journal of Geophysical Research: Atmospheres*, 114, 2009.

634 [Swap, R., Garstang, M., Greco, S., Talbot, R., and Källberg, P.: Saharan dust in the Amazon Basin, \*Tellus B\*, 44, 133–149, 1992.](#)

635 [Taghavi, F. and Asadi, A.: The Persian Gulf 12th April 2007 dust storm: observation and model analysis, in: EUMETSAT Meteorological  
636 Satellite Conference, Darmstadt, Germany, pp. 8–12, 2008.](#)

637 Tanaka, T. Y., Kurosaki, Y., Chiba, M., Matsumura, T., Nagai, T., Yamazaki, A., Uchiyama, A., Tsunematsu, N., and Kai, K.: Possible  
638 transcontinental dust transport from North Africa and the Middle East to East Asia, *Atmospheric Environment*, 39, 3901–3909, 2005.

639 Tegen, I., Schepanski, K., and Heinold, B.: Comparing two years of Saharan dust source activation obtained by regional modelling and  
640 satellite observations, *Atmospheric Chemistry and Physics*, 13, 2381–2390, 2013.

641 Teller, A. and Levin, Z.: The effects of aerosols on precipitation and dimensions of subtropical clouds: a sensitivity study using a numerical  
642 cloud model, *Atmospheric Chemistry and Physics*, 6, 67–80, 2006.

643 Thomson, M. C., Molesworth, A. M., Djingarey, M. H., Yameogo, K., Belanger, F., and Cuevas, L. E.: Potential of environmental models to  
644 predict meningitis epidemics in Africa, *Tropical Medicine & International Health*, 11, 781–788, 2006.

645 Tsamalis, C., Chédin, A., Pelon, J., and Capelle, V.: The seasonal vertical distribution of the Saharan Air Layer and its modulation by the  
646 wind, *Atmospheric Chemistry and Physics*, 13, 11 235–11 257, 2013.

647 Tulet, P., Mallet, M., Pont, V., Pelon, J., and Boone, A.: The 7–13 March 2006 dust storm over West Africa: Generation, transport, and  
648 vertical stratification, *Journal of Geophysical Research: Atmospheres*, 113, 2008.

649 Vuolo, M. R., Chepfer, H., Menut, L., and Cesana, G.: Comparison of mineral dust layers vertical structures modeled with CHIMERE-DUST  
650 and observed with the CALIOP lidar, *Journal of Geophysical Research: Atmospheres*, 114, 2009.

651 Wagener, T.: Le fer à l’interface océan-atmosphère: Flux et processus de dissolution dans l’eau de mer., Ph.D. thesis, Université de la  
652 Méditerranée-Aix-Marseille II, 2008.

653 Wang, M., Bailey, S., Pietras, C., McClain, C., and Riley, T.: SeaWiFS aerosol optical thickness matchup analyses, The Sea-WiFS Postlaunch  
654 Technical Report Series, 10, 39–44, 2000.

655 [Weinzierl, B., Ansmann, A., Prospero, J., Althausen, D., Benker, N., Chouza, F., Dollner, M., Farrell, D., Fomba, W., Freudenthaler, V., et al.:  
656 The Saharan Aerosol Long-range Transport and Aerosol-Cloud-Interaction Experiment \(SALTRACE\): overview and selected highlights,  
657 \*Bulletin of the American Meteorological Society\*, 2016.](#)

658 Winker, D.: Accounting for multiple scattering in retrievals from space lidar, in: Proc. of SPIE Vol, vol. 5059, p. 129, 2003.

659 Winker, D. M., Hostetler, C., Vaughan, M., and Omar, A.: CALIOP Algorithm Theoretical Basis Document, Part 1: CALIOP Instrument,  
660 and Algorithms Overview, Release, 2, 29, 2006.

661 Winker, D. M., Hunt, W. H., and McGill, M. J.: Initial performance assessment of CALIOP, *Geophysical Research Letters*, 34, 2007.

662 Wu, M.-L. C., Reale, O., Schubert, S. D., Suarez, M. J., Koster, R. D., and Pegion, P. J.: African easterly jet: structure and maintenance,  
663 *Journal of Climate*, 22, 4459–4480, 2009.

664 Yang, W., Marshak, A., Várnai, T., Kalashnikova, O. V., and Kostinski, A. B.: CALIPSO observations of transatlantic dust: vertical stratifi-  
665 cation and effect of clouds, *Atmospheric Chemistry and Physics*, 12, 11 339–11 354, 2012.



666 Yu, H., Chin, M., Winker, D. M., Omar, A. H., Liu, Z., Kittaka, C., and Diehl, T.: Global view of aerosol vertical distributions from CALIPSO  
667 lidar measurements and GOCART simulations: Regional and seasonal variations, *Journal of Geophysical Research: Atmospheres*, 115,  
668 2010.

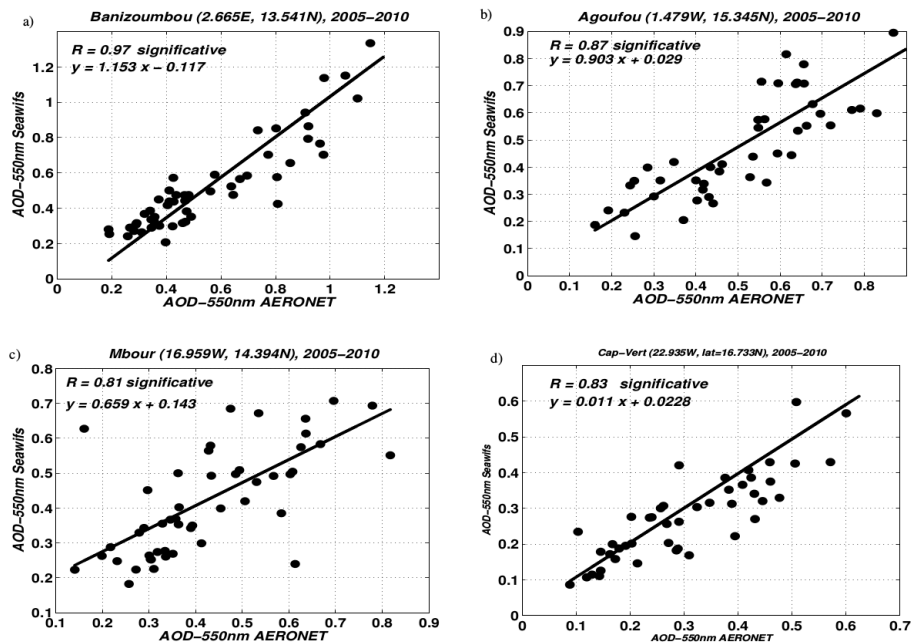


**Figure 1.** Comparison of monthly mean aerosol optical depth (AOD) between SeaWiFS (550 nm) and ground measurements from AERONET (675 nm) from January 2005 to December 2010. This comparison is done at the following stations : a) Banizoumbou (53 points), b) Agoufou (47 points), c) M'bour (50 points) and d) Cape verde (47 points). The red solid line represents the regression between both dataset

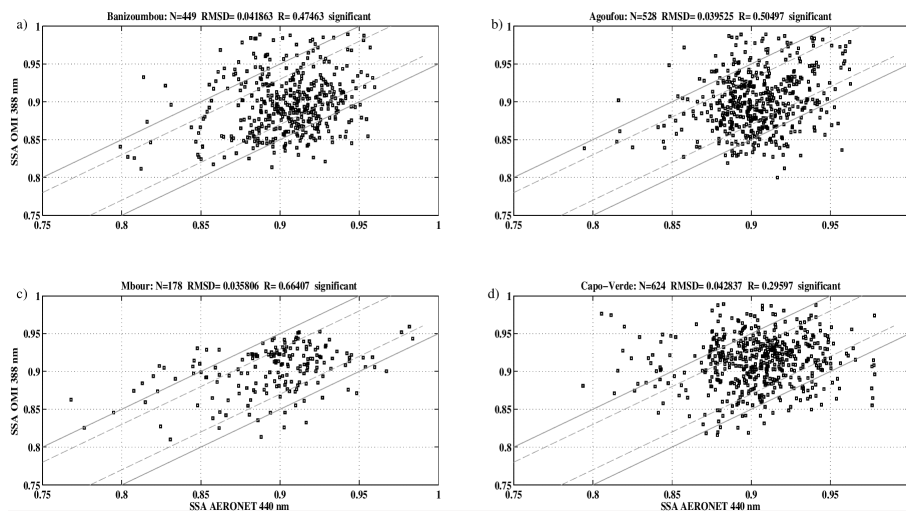


**Figure 2.** OMAERUV SSA at 440–388 nm wavelength as a function of AERONET SSA at 440 nm at a) Banizoumbou (lon=2.665E, lat=13.541N; a total of 449 retrievals are plotted, yielding a root-mean-square difference (RMSD) of 0.04); b) Agoufou (lon=-1.4791, 479W, lat=15.345N; 528 retrievals with a RMSD of 0.04); c) M'bour (lon=-16.95916, 959W, lat=14.394N; 178 retrievals with a RMSD of 0.04) and d) Capo Verde (lon=-22.93522, 935W, lat=16.733N; 624 retrievals with a RMSD of 0.04). The solid lines indicate the domain where the two retrievals agree with each other within 0.03 and the dashed lines indicate agreement within 0.05. The AERONET's data used here are Level-2, quality-assured for Banizoumbou, Agoufou and M'bour sites. For Cape Verde Level-1.5, is used to get a significant number of retrievals.

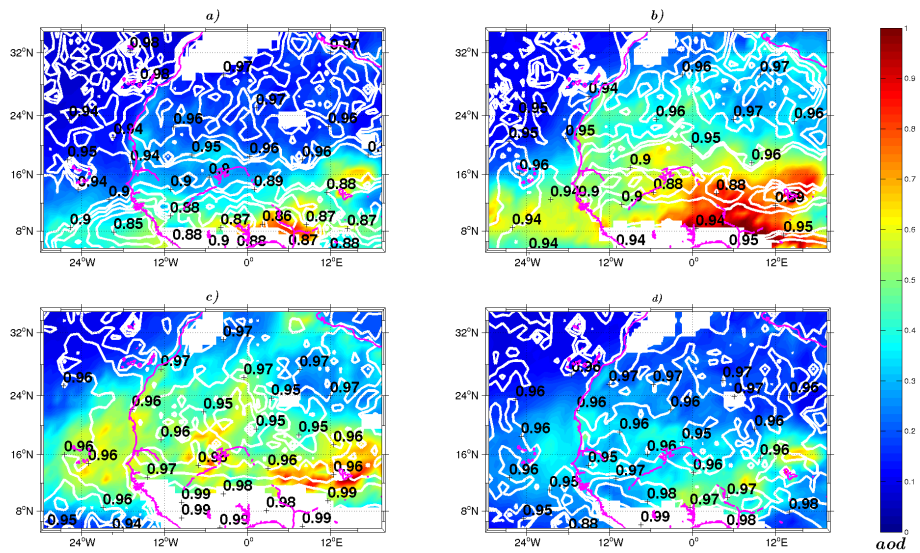


**Figure 3.** Seasonal distribution of aerosol optical depth (average between 2005 and 2010) at 550 nm wavelength (colours) from SeaWiFS for a) winter (DJF); b) spring (MAM); c) summer (JJA) and d) fall (SON). Single scattering albedo (SSA) from OMI is superimposed with white contour lines. The box delimited by brown dashed lines represent the band of latitude averaged in Fig. 4 ( $12^{\circ}$ - $21^{\circ}$ N) where dust aerosols have the strongest contribution to AOD.

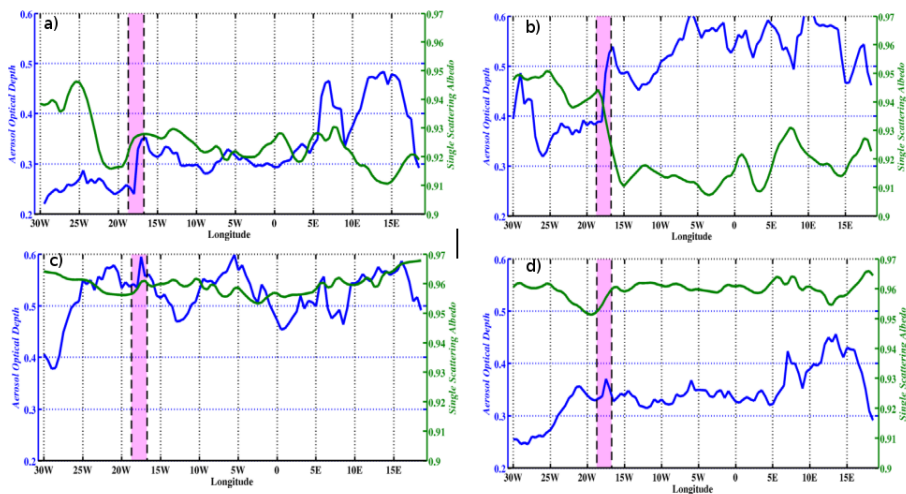


**Figure 4.** Seasonal SeaWiFS AOD at 550 nm (bleu), Aura/OMI SSA (green) zonally averaged between  $12^{\circ}$  and  $21^{\circ}$ N and from 2005 to 2010: a) DJF; b) MAM; c) JJA; and d) SON. The black dashed lines indicate the continent-ocean transition for the latitude range  $12^{\circ}$ - $21^{\circ}$ N.

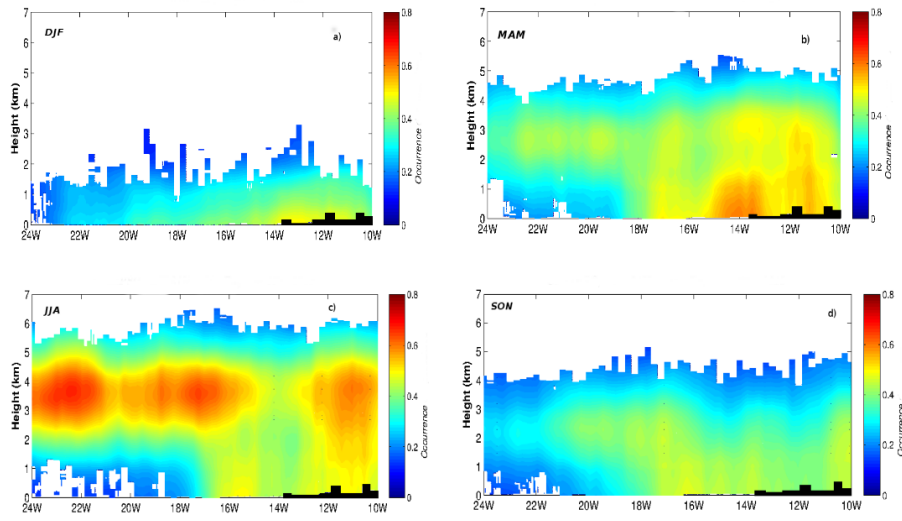


**Figure 5.** CALIOP daytime seasonal vertical distribution of the frequency of mineral dust aerosol occurrence zonally averaged between 12° and 21°N over the period 2007-2013: a) winter; b) spring; c) summer; and d) fall.

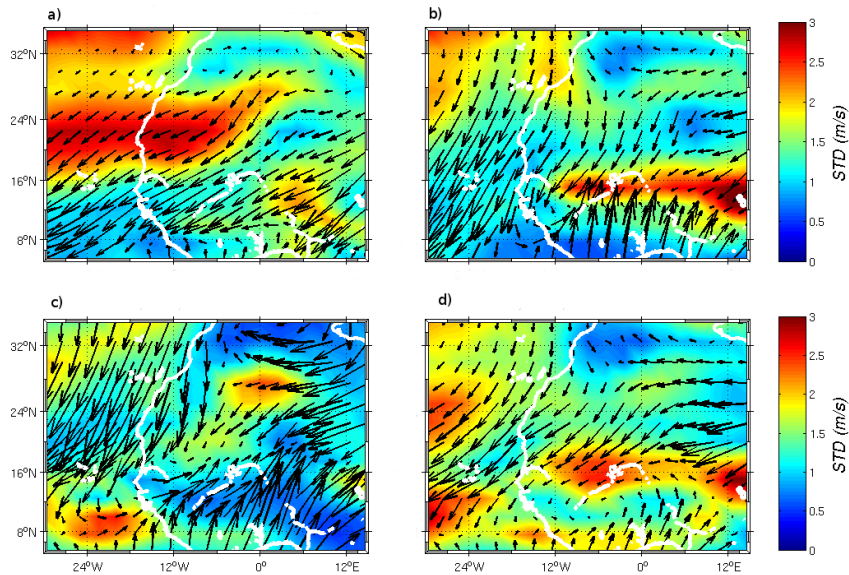


**Figure 6.** Seasonal mean zonal wind field at 925 hPa over West Africa from NCEP Reanalysis between 2000 and 2012: a) winter (DJF); b) spring (MAM); c) summer (JJA); and d) fall (SON). The vectors show wind direction while colors indicate the standard deviation of wind velocity ( $\text{m}\cdot\text{s}^{-1}$ ).

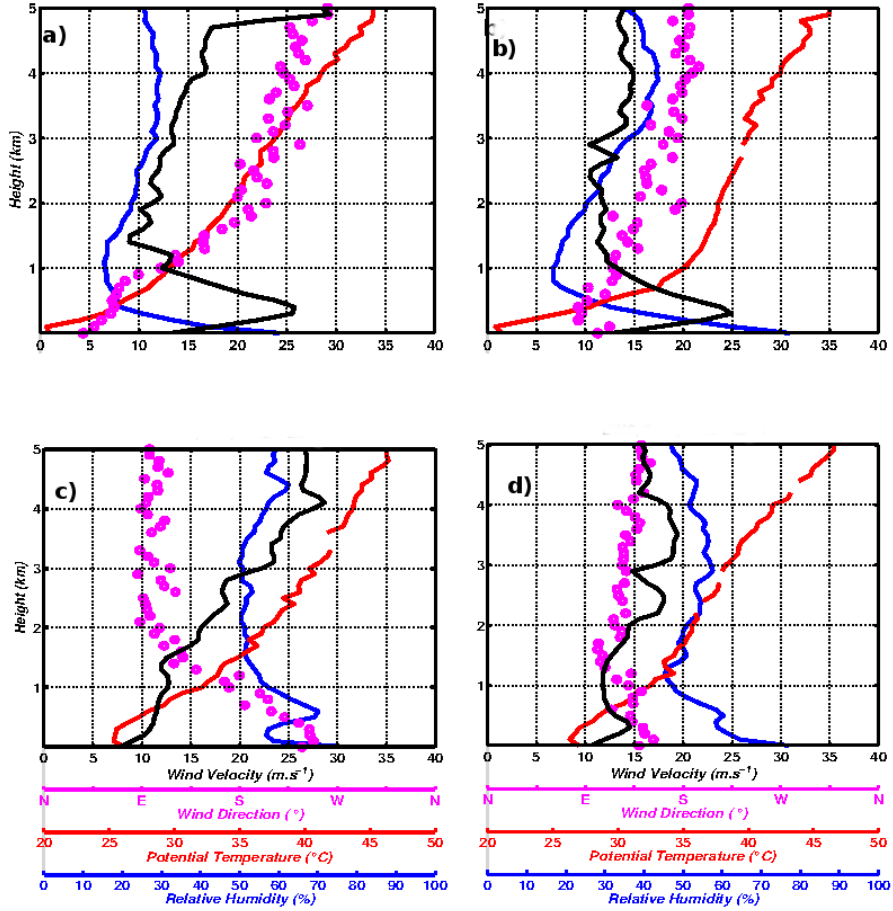


**Figure 7.** Mean seasonal vertical profiles of wind velocity (black line), wind direction (pink dots), potential temperature (red line) and relative humidity (blue line) at Dakar weather station (14.73°N, 17.51°W) for a) winter; b) spring; c) summer; and d) fall. Observations correspond to weather balloon launched daily at 12UTC for years 2012 to 2014.